FEM-BASED METHOD FOR THE SIMULATION OF DIELECTRIC WAVEGUIDE GRATING BIOSENSORS

Thomas Guillod[1], Florian Kehl[2, 3, 4, *], and Christian Hafner[1]

[1]Laboratory for Electromagnetic Fields and Microwave Electronics, Swiss Federal Institute of Technology, Zürich CH-8092, Switzerland

[2]Laboratory of Biosensors and Bioelectronics (LBB), Swiss Federal Institute of Technology, Zürich CH-8092, Switzerland

[3]CSEM Centre Suisse d'Electronique et de Microtechnique SA, Landquart CH-7302, Switzerland

[4]Optics Balzers AG, Balzers FL-9496, Liechtenstein

Abstract—Label-free optical biosensors are important tools to study the kinetics, interaction and presence of (bio) chemical compounds in various fields such as biotechnology, pharma, diagnostics as well as environmental and food quality monitoring. Systems based on planar optical waveguides with input/output grating couplers are of interest as they offer multiple tuning parameters for the chip design and their high sensitivity. In the present paper, an algorithm based on the Finite-Elements Method (FEM) is proposed for finding the chip response and optimizing the sensitivity of the sensor system. Total field and scattered field coupled with the Transmission Line Transfer Matrix Method (TLTMM) are compared for the FEM. Unlike some widely used approximations, the impact of the grating depth, shape, duty cycle as well as losses and surface roughness are taken into account. Another advantage of the presented method is the possibility to implement a large part of the algorithm with commercially available FEM solver. Several practical situations are treated proving the validity of the approach against the Local Interference Method (LIME). The waveguide losses appear to be a decisive parameter for the chip design.

1. INTRODUCTION

In the last decade, the use of chemical and biological sensors, based on electromagnetic waves at optical wavelengths has grown significantly. A particularly interesting category of optical biosensor is based on waveguides with a high refractive index film. The sensing action is accomplished by the changes of the effective refractive index, sensed by the evanescent field. This technique has found applications for label-free as well as for fluorescent-label sensors.

Different configurations for label-free waveguide based sensor are possible [1–3]. The dielectric waveguide with input/output grating coupler is one of the simplest and cheaper solutions. Many tuning parameters can be used for the design of the chip in order to reach a high sensitivity and thus this configuration will be investigated further in this paper. Only the electromagnetic modeling of the waveguide will be considered, the biochemical modeling can be found in [3].

The chip is a simple multilayer planar dielectric waveguide. On a substrate (mostly glass) a thin film with a high refractive index is added (in general Tantalum Pentoxide Ta_2O_5). On the film, the biological layer (sensing layer) and the cover (mostly aqueous solution) are placed. The cover and the substrate form the cladding of the waveguide. The resulting sensor chip is shown in Figure 1 with the important geometry and material parameters. The waveguide thickness is not the same for the input and output coupler for preventing interference between the input and output beams which occurs if the coupling angles are the same [3, 4]. The dimensions in the x and z directions are much larger than the grating period. This means that it is possible to consider the grating as a two-dimensional periodic geometry.

The input pad is illuminated with a laser. There are two possible operation modes with this kind of chip [2]. The first is the angular tuning where the input angle θ_{in} is varied and the intensity (eventually also the position) of the output beam is measured at a constant wavelength. The coupling angle is where the intensity is maximal. Then any changes of the refractive index or the thickness of the sensing biolayer lead to a change of the coupling angle of the input grating pad and can be detected. Alternatively it is also possible to measure the transmitted light at the cover side. When the coupling condition is fulfilled, the energy goes into the film and a minimum can be observed at the cover. The second operation is the so called WIOS principle (wavelength interrogated optical sensor) [3, 4]. The angle of the incident beam is maintained constant while the wavelength is changed (by some nanometers), while the intensity of the output beam

is measured. Any change of the effective refractive index, e.g., due to the adsorption of biomolecules to the sensor surface, the resulting resonance curve shift will be monitored. In the following, only the angular interrogation will be investigated, mainly due to practical means like extended tuning range as well as stability and independence of the wavelength of the laser source. Nonetheless, the following calculations would also hold true for the wavelength interrogating sensing scheme.

The design of a biosensor obeys to some basic principles described in [2]. The sensitivity should be maximal in order to have a small detection limit. The signal to noise ratio is clearly another important factor, strongly influenced by the so called SBSR (sensing layer to bulk volume signal ratio) and defined as the sensitivity with respect to the sensing layer over the sensitivity with respect to the cover [5]. In the following, the focus will be on the grating coupler and not on a complete chip. There is a duality relation between an input and an output coupler such that the results are valid for both cases. Because for many waveguide grating configurations, including the one presented in Figure 1, the TM_0 mode leads to higher sensitivity [6] and a sharper resonance curve, it will be investigated in this work. Even though the waveguide's first mode would be TE_0, its sensitivity is inferior to the TM_0 mode, implying that the TE_0 mode is only useful if this is the unique existing mode due to the layer's thickness or if two linearly independent measurements are required [7]. The presented methods work both for TE and TM polarization.

For the prediction of the sensor sensitivity, different methods are known such as analytical approximation based on the mode equation [7] or methods based on rigorous diffraction theory [6]. In [8], Cottier et al. have introduced the Local Interference Method (LIME), which is a simplified multiple scattering method [9]. This method has proven to be very fast but the used implementation suffers of many limitations. The computation relies on a thin grating approximation thus it is not possible to take into account the exact grating shape, its duty-cycle nor depth. The waveguide film losses are also neglected. These simplifications do not allow to find the resonance curve of the sensor, particularly the finite width half maximum.

The paper presents an algorithm based on Finite-Elements Method (FEM) and Transmission Line Transfer Matrix Method (TLTMM) for computing the field distribution and extracting the sensitivity of the chip. This method allows the inclusion of the grating depth, duty-cycle and shape, the film losses due to damping, the surface roughness, etc.. The simulation of non-periodic, non-uniform gratings has also been done but will not be presented here. The main

advantage of FEM is the flexibility and the availability of powerful commercial solvers. Consequently the implementation of the described method is particularly fast and the simulation of other configurations is possible with small adaptations. After the presentation of the numerical methods and the validation against LIME, some results are for illustrating the influence of the film thickness, the grating depth and the film losses.

2. NUMERICAL METHODS

2.1. FEM Total Field

The input coupler as shown in Figure 1 can be simplified into a periodic structure as presented in Figure 2(a). The goal is to find the electromagnetic field distribution with a plane wave excitation. Periodic boundary conditions are introduced with Floquet periodicity. The x component of the wave vector k_x is constant at the interface between the materials and can be used without any problem for the periodicity.

The main problem is to find boundary conditions that allow the injection of the plane wave and the absorption of the reflected and diffracted waves. Starting from the grating equations [10, 11]:

$$m \cdot \lambda_0 = \Lambda_l \cdot (n_c \sin(\alpha_m) - n_s \sin(\theta)) \tag{1a}$$

$$m \cdot \lambda_0 = \Lambda_l \cdot n_s \cdot (\sin(\theta_m) - \sin(\theta)) \tag{1b}$$

with m representing the different grating diffraction orders. The
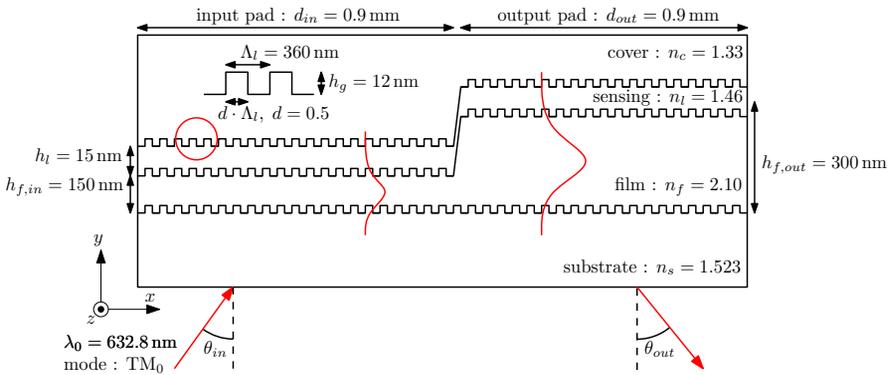
Figure 1. Biosensor waveguide chip with an input and an output grating coupler.

existence of the diffraction is ruled by the following equation:

$$-(n_s + n_c) \; < \; \frac{m \cdot \lambda_0}{\Lambda_l} < (n_s + n_c) \tag{2a}$$

$$-2 \cdot n_s \; < \; \frac{m \cdot \lambda_0}{\Lambda_l} < 2 \cdot n_s \tag{2b}$$

Note that this condition is conservative since the incidence angle is not taken into account. Then Equation (1) can be solved for the angle θ_m and α_m and thus the wave vectors for the different orders are easily obtained at the substrate and at the cover with:

$$k_s \; = \; k_0 \cdot n_s \tag{3a}$$

$$k_{m,s,x} \; = \; k_s \cdot \sin(\theta_m) \tag{3b}$$

$$k_{m,s,y} \; = \; k_s \cdot \cos(\theta_m) \tag{3c}$$

$$k_c \; = \; k_0 \cdot n_c \tag{4a}$$

$$k_{m,c,x} \; = \; k_c \cdot \sin(\alpha_m) \tag{4b}$$

$$k_{m,c,y} \; = \; k_c \cdot \cos(\alpha_m) \tag{4c}$$

Finally these waves are represented in the FEM model with port boundary conditions [12]. A port boundary condition can inject an electromagnetic wave with a given field distribution and propagation constant. Further, a port can also absorb the waves that have the same propagation constant. Since the propagation constants are different for each diffraction order, a port is needed at the cover and substrate for each order m (and $-m$). The electric field at the port and
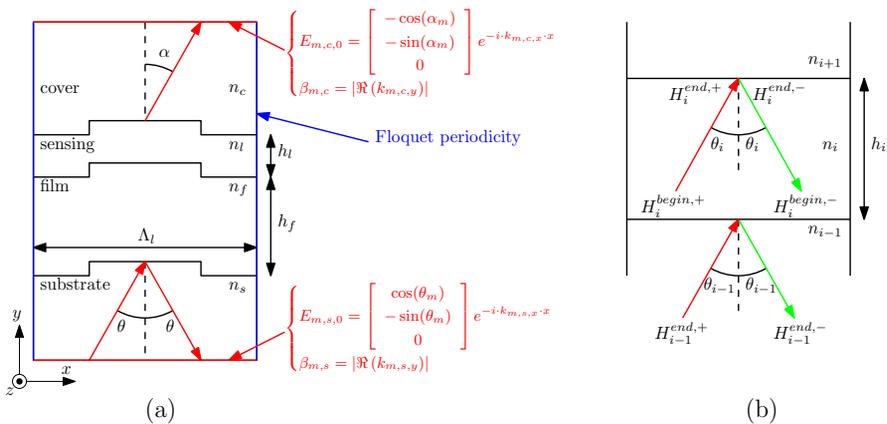
Figure 2. Considered geometry for FEM with TM waves.

the propagation constant are set with the following equation for a transversal magnetic wave (see Figure 2(a)):

$$
\begin{cases}
E_{m,s,0} = \begin{bmatrix} \cos(\theta_m) \\ -\sin(\theta_m) \\ 0 \end{bmatrix} e^{-i \cdot k_{m,s,x} \cdot x} \\
\beta_{m,s} = |\Re(k_{m,s,y})|
\end{cases}
\tag{5}
$$

$$
\begin{cases}
E_{m,c,0} = \begin{bmatrix} -\cos(\alpha_m) \\ -\sin(\alpha_m) \\ 0 \end{bmatrix} e^{-i \cdot k_{m,c,x} \cdot x} \\
\beta_{m,c} = |\Re(k_{m,c,y})|
\end{cases}
\tag{6}
$$

Only the direction of the field is considered. The amplitude is scaled such that a given amount of power is injected through the boundary. Only the port with the diffraction order 0 at the substrate side has a non-zero power. This corresponds to the plane wave that models the laser that illuminates the grating.

The main advantage with the FEM is that a solution of the wave equation is searched for the real chip geometry which is not the case for the local interference approximation. This allows taking into account more parameters such as the grating depth and duty cycle. The number of layers in the stack has no influence on the method, and it is possible to model an arbitrary grating shape. It is also possible to include materials with losses or metallic gratings [13]. From the ports the scattering matrix and thus the reflection and transmission coefficients can be directly extracted. The limitations of the total field FEM formulation comes mainly from the computational cost. Problems also occur if a lot of diffraction orders are present in the simulated geometry.

2.2. FEM Scattered Field

For problems with plane wave excitation it is often easier to write a scattered field formulation of the finite element method [14]. For a dielectric stacked grating a plane wave cannot be used for the background field. The background field should contain the solution for the stack with planar interfaces between the materials (without the grating). Then the grating rectangles are added and the scattered field is solved again with Floquet periodicity but with PMLs at the top of the cover and at the bottom of the substrate.

A possibility for obtaining the background field is to use the FEM as described in Section 2.1. Since the interface is plane, only the diffraction order 0 is needed. A better and faster solution is to find an analytical solution with the Transmission Line Transfer Matrix Method (TLTMM). The implementation of TLTMM is based on [15, 16] which allows losses.

With Snell's law, the angle, the wave impedance and the component of the wave vector can easily be computed in each layer. The used notations are described in Figure 2(b). One can see that there is a forward and a backward travelling wave in each layer. Now the propagation of the wave inside a layer can be described with a amplitude transfer matrix:

$$\left[\begin{array}{c} H_i^{\mathrm{end},+} \\ H_i^{\mathrm{end},-} \end{array} \right] = L_i \cdot \left[\begin{array}{c} H_i^{\mathrm{begin},+} \\ H_i^{\mathrm{begin},-} \end{array} \right] \tag{7}$$

At the interface between two adjacent layers, the reflection coefficient should be considered in both directions. The matrix $I_{i,i-1}$ contains the reflections and transmission coefficients:

$$\left[\begin{array}{c} H_i^{\mathrm{begin},+} \\ H_i^{\mathrm{begin},-} \end{array} \right] = I_{i,i-1} \cdot \left[\begin{array}{c} H_{i-1}^{\mathrm{end},+} \\ H_{i-1}^{\mathrm{end},-} \end{array} \right] \tag{8}$$

Finally, it is possible to assemble all the propagation and discontinuity transfer matrices in order to write an equation system for a stack of N dielectrics:

$$\left[\begin{array}{c} H_N^{\mathrm{end},+} \\ 0 \end{array} \right] = T \cdot \left[\begin{array}{c} H_1^{\mathrm{begin},+} \\ H_1^{\mathrm{begin},-} \end{array} \right] \tag{9}$$

$$T = L_N \cdot I_{N,N-1} \cdot L_{N-1} \cdot \ldots \cdot L_2 \cdot I_{2,1} \cdot L_1 \tag{10}$$

where $H_1^{\mathrm{begin},+}$ is the given plane wave excitation, and $H_1^{\mathrm{begin},-}$ and $H_N^{\mathrm{end},+}$ are the unknown variables. Per definition there is no reflection at the last layer which implies $H_N^{\mathrm{end},-} = 0$. With the help of the matrix equation the field distribution in the complete structure can be found recursively with the help of the Equations (7) and (8). With Maxwell's equations all the fields (B, E, etc.) can be also found. It is also possible to extract the Poynting vector and the absorption. The combined analytical (TLTMM) and numerical (FEM) is a very flexible and powerful method for simulating diffraction gratings. It is possible to take into account the material losses or to include metallic shields (with a higher computation time). This inclusion of anisotropic materials is conceivable. There is also no limitation for the grating shape. It is also possible to extend the procedure for a non-periodical grating or for a grating with an excitation that is not a plane wave.

3. COMPARISON BETWEEN THE METHODS

3.1. Detection of the Coupling

The presented methods will be compared against LIME for a reference grating (see input pad parameters in Figure 1). The FEM with total field formulations can be either modeled with ports at the cover or with a PML.

For FEM, different angles are scanned in order to find the angle with the best coupling. For a biosensor the goal is to bring the maximum amount of energy in the sensing layer (where the biochemical reaction takes places) [7]. Since the mode is guided in the film, the energy in the film is another choice. Another possibility is to minimize the transmission coefficient from the substrate to the cover if illuminated from the former side. The energy is measured at the cover side with a CMOS or CCD sensor. When the transmission is minimal, this means that the energy is coupled into the waveguide. With the total field formulation this can be obtained directly from the scattering matrix between the ports. For a single mode waveguide the S-parameters can be interpreted in the term of power flow [14]:

$$E_{\text{domain,abs}} = \iint_{\text{domain}} W_{\text{avg}}\, dS \tag{11a}$$

$$E_{\text{domain,rel}} = \frac{\iint_{\text{domain}} W_{\text{avg}}\, dS}{\iint_{\text{all}} W_{\text{avg}}\, dS} \tag{11b}$$

$$T_i = \left| S_{21}^2 \right| \tag{11c}$$

$$= \frac{\text{power transmitted at cover side (order } i)}{\text{incident power at substrate side}} \tag{11d}$$

where W_{avg} is the averaged energy density over a time period. For comparing the absolute energy density between total and scattered field, the curves should be normalized.

The resulting resonance curve for total field FEM can be seen in Figure 3 for the different expressions shown in Equation (11). One can see that there is almost no difference between measuring the resonance with transmission coefficient, relative or absolute energy (less than $0.002°$ error). The deviation between the maximum becomes smaller with decreasing grating depth.

The main difference arises from the full width half maximum. The peak width is only about $0.001°$ for the transmission coefficient and for the absolute energy and about $0.08°$ for the relative energy. The narrow peak is the measured peak (the transmitted/coupled energy is measured). But the relative energy is also useful because the peak is easier to detect with numerical maximization routines.
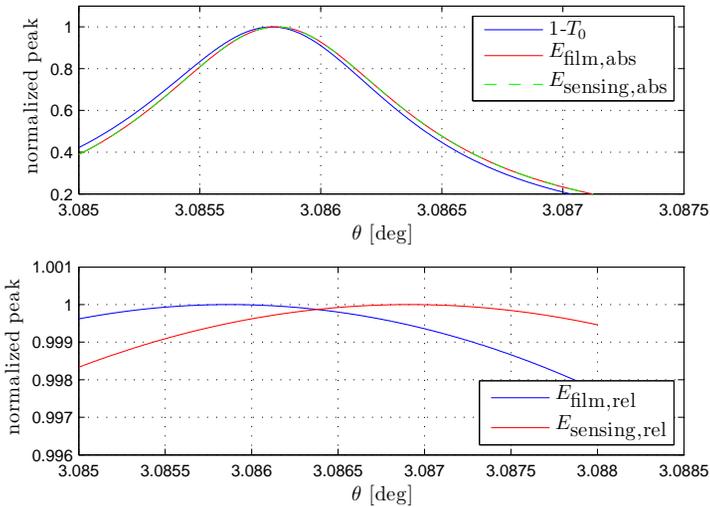
Figure 3. Resonance curves with total field FEM formulation (small scale).

A comparison between total field and scattered field formulations has also been performed. Since the fields did not have the same amplitude, it is better to make the comparison with the relative energy. It can be concluded that in this case the deviation between the total and scattered field FEM formulations is lower than 0.01% for $E_{\text{film,rel}}$ and $E_{\text{sensing,rel}}$ over the whole angular range.

3.2. Comparison between FEM and LIME

Since the used implementation of LIME is only valid for thin gratings, the comparison has been done from a grating depth of $25\,\text{nm}$ to $0.25\,\text{nm}$. In the upper plot of Figure 4, the resonance curves are shown for smaller grating depths (relative energy in sensing layer). The lower plots show the error of the resonance angle between LIME and FEM (scattered field and total field). The black line (in the lower plots) represents the maximum resolution (distance between two computed angles) which represents the minimum reachable error with the used angular sweep.

With a grating depth of $0.25\,\text{nm}$ the error is clearly smaller than $10^{-5\circ}$ and seems to remain stable. Simulations with a smaller grating depth are hard to perform because the mesh is becoming too large. This precision is clearly sufficient for the design of a biosensor. The conclusion is that the different finite element models are in good agreements and that for a simple geometry with a thin grating the
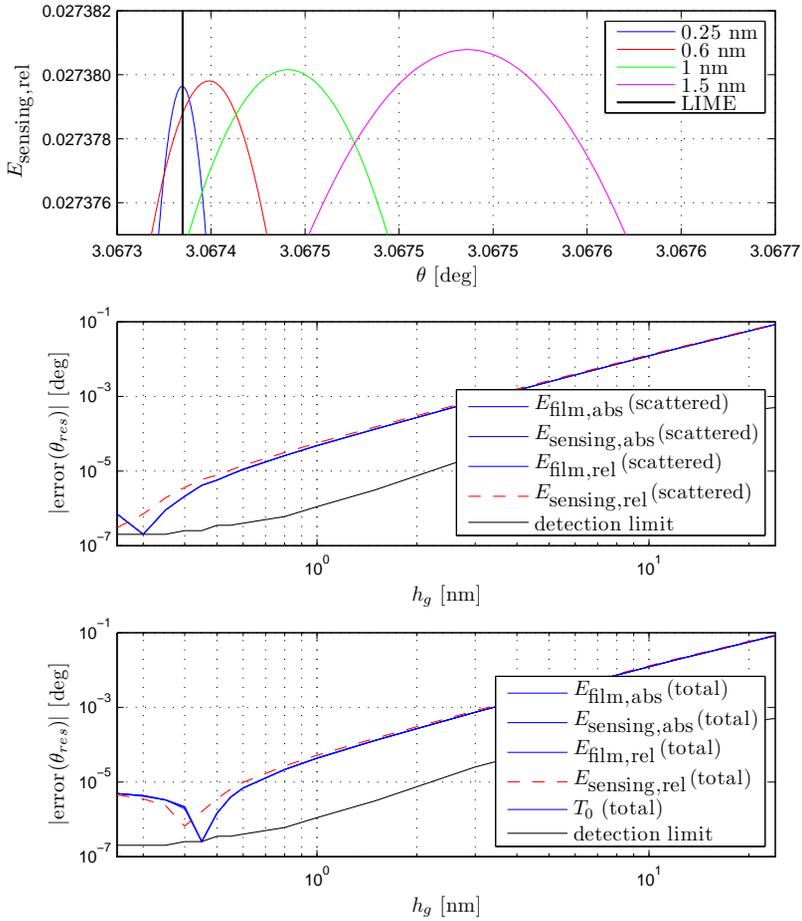
Figure 4. Influence of the grating depth on the error between FEM and the local interference method.

LIME has proven to be sufficient regarding the coupling angle. In particular the LIME should not be used if the grating depth is greater than 15 nm.

4. SENSOR SENSITIVITY

4.1. Procedure for Finding the Resonance

In Section 3, the resonance curves of the energy in the sensing layer have been obtained with an angular sweep. But if only the

angle of resonance is needed, it is clear that this solution is not optimal. A standard minimization algorithm can be used (for example Nelder-Mead simplex) to find the resonance, but here a model-based optimization has been used. From the grating theory it is known that for the given configuration, the resonance curve is a Lorentzian function [6, 17]. From the symmetry of the geometry it is clear if there is a resonance peak at $\theta_{\rm res}$, there is the same peak at $-\theta_{\rm res}$. Consequently, the two peaks should be considered together. Another effect comes from the fact that even at a point far away from the resonance the energy in the sensing layer is not zero. Thus an offset should also be included in the function. Including these two facts, a fit function is constructed:

$$E_{\rm fit}(\theta) = \frac{f_{\max}\left(\frac{fwhm}{2}\right)^2}{(\theta - \theta_0)^2 + \left(\frac{fwhm}{2}\right)^2} + \frac{f_{\max}\left(\frac{fwhm}{2}\right)^2}{(\theta + \theta_0)^2 + \left(\frac{fwhm}{2}\right)^2} + \text{offset} \quad (12)$$

where $fwhm$ is the full width half maximum. The function is fitted at the least square sense with the computed points and the maximum position, the peak value and the full width half maximum can be extracted. Note that the maximum of the sum of the two peaks (Equation (12)) is no more at θ_0 (but at $\theta_{\rm res}$) and that the maximum value is not $f_{\max}$.

The validity of the chosen fit function is shown in Figure 5. The geometry has been chosen (adaptation of the film thickness) such that
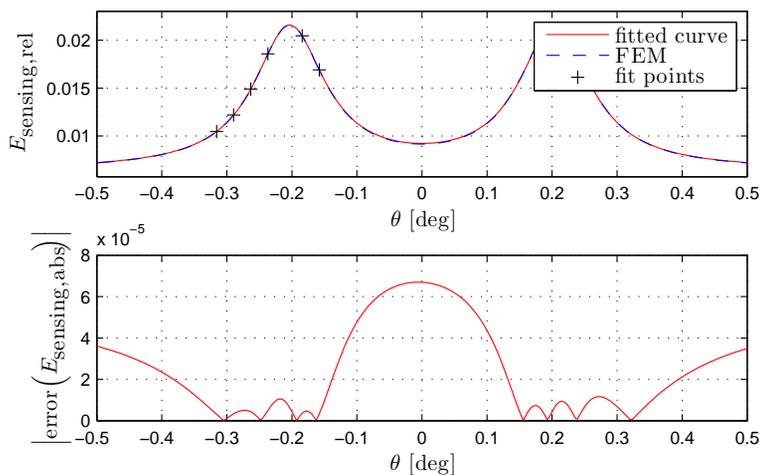
Figure 5. Comparison of the resonance peak computed with FEM and the fitted curve.

the resonance angle is very small (about $0.2°$). The obtained curve makes clear the choice of the sum of the two Lorentzian peaks with maxima at $\pm\theta_0$ done in Equation (12).

The dashed blue curve is computed with FEM at a lot of different angles. The black points are the data used for the least square fit and the fitted function is the red curve. The lower plot shows the error between the fit and the reference curve obtained directly with FEM. One can see that a very low number of points is sufficient for reconstructing the shape of the resonance peak with a good accuracy. An advantage of the model-based search is that not only the value and position of the extremum is given but also an estimation of the complete peak shape. For example the full width half maximum is an important parameter for the sensor in order to find its Q-factor.

4.2. Computation of the Sensitivity

Finding the resonance angle or frequency is important but not sufficient for designing a grating based biosensor. The sensitivity of the sensor is defined as

$$G_{\text{sensitivity}} = \frac{\Delta \text{ measurement parameter}}{\Delta \text{ sensing parameter}} \tag{13}$$

where the sensitivity parameter is the parameter that is wanted, an example can be the bindings of the molecules. But here only the parameters of the waveguide are considered. Consequently the sensitivity parameter will be the thickness or the refractive index of the sensing layer. The measurement parameter is the angle or the frequency for respectively angular and wavelength scan. The goal is to maximize the sensitivity G of the sensor in order to reach a low detection limit. Other transfer functions can be considered such as the signal-to-noise ratio or the disturbance rejection. An interesting case is the signal to noise ratio, for example the SBSR (sensing layer to bulk volume signal ratio) [5]:

$$G_{\text{SBSR}} = \frac{\frac{\partial \theta}{\partial n_l}}{\frac{\partial \theta}{\partial n_c}} \tag{14}$$

Any changes of the refractive index of the cover are considered as noise. The goal is to have a large sensitivity for the sensing layer and a small one for the cover. The SBSR can also be written for changes of the sensing layer thickness. This means that a derivative should be computed. This is done numerically with a first, second or fourth order approximation. The Richardson's formulas have been used to estimate the required step size [18]. The second order approximation

has proven to be sufficient. For finding the maximum, again the procedure of Figure 5 is used for all the steps of the sensitivity parameter needed for the numerical approximation of the derivative (see Equation (13)). Often the sensitivity is expressed for the effective refractive index [5, 7, 19] but here the sensitivity is directly expressed with the measurement parameter. This gives a direct insight on the practical signification of the results.

The method described above can be used to find the response of a particular sensor. Since the goal is to optimize the design, a geometry or a material parameter (here called optimization parameter) is varied and the response is computed for each value. From the obtained results, the sensor design can be improved. The optimization parameter can be specified in a table and the sensitivity is computed for all the given values. If the optimization should be done with more than one parameter then the computation costs are too high with multi-dimensional table and a genetic or direct search algorithm is used for finding the optimal design. The direct search algorithm has proven to be well suited for optimization with one to three variables. A strongly
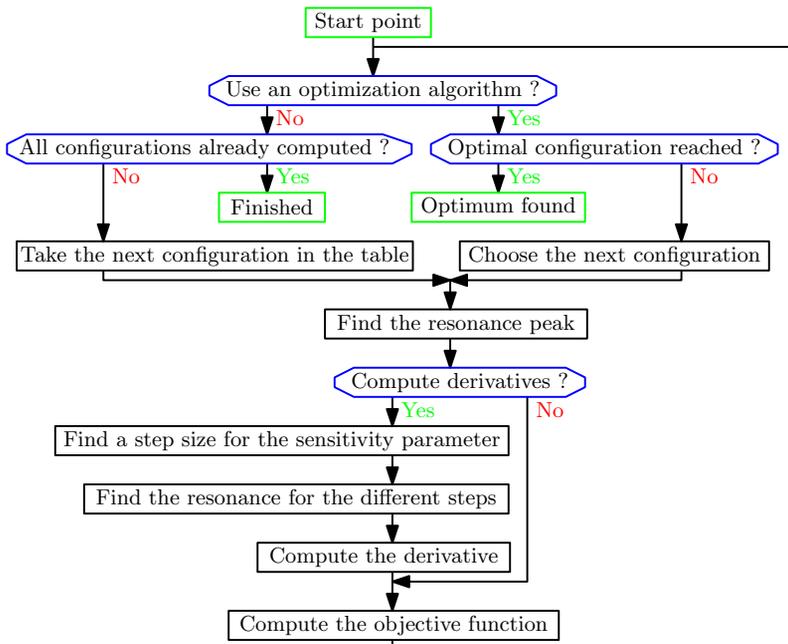
Figure 6. Simplified flow chart for finding the optimal sensor sensitivity.

simplified flow chart of the algorithm used to find an optimal biosensor is shown in Figure 6. The objective function can be a simple expression as in Equation (13) or a more complex one as in (14).

5. RESULTS

5.1. Film Thickness

The study of the impact of the film thickness h_f is probably one of the most studied parameter for waveguide grating based biosensors [3, 5–8]. Thus this type of simulation can be used as validation for the proposed method. The used parameters can be found in Figure 1. The film is varied from 90 nm to 254 nm. For all the geometries, the resonance angle (peak position), the peak value (amplitude of the peak), and the derivative of the angle with respect to the refractive index of the sensing layer are computed. The results for the position of the resonance and for the derivative are then compared between FEM and LIME in Figure 7. The relative energy is the sensing layer has been maximized ($E_{\text{sensing,rel}}$, see Equation (11)) for finding the resonance condition (total field FEM). The small differences for the resonance angle can be explained by the fact that the finite grating depth is neglected for the local interference method. The error near the cutoff thickness is becoming bigger. This comes from the fact that the LIME uses a very basic cutoff model (the waveguide is taken without the grating as a normal slab dielectric waveguide).

The lower plot is the sensitivity $\frac{\partial \theta_{\text{res}}}{\partial n_l}$ which represents the measured change of the coupling condition for a change in the biological sensing layer. For the given parameters, the relative energy is maximal for a film thickness of 121 nm and the sensitivity has a local maximum at 140 nm, implying that the sensitivity is not maximal where the energy is maximal. Again there are some differences near the cutoff due to the lack of accuracy of the LIME in this region. In the other regions, the difference between FEM and LIME is less than 1% which means that LIME is sufficient if the angle is not near the normal incidence, the film thickness is not near the cutoff and if the grating is thin. Similar results can be found in [3, 5, 7] and thus this indicates that the proposed method for computing the sensitivity with FEM is valid.

The peaks near 186 nm (in Figure 7) are placed where the incidence angle is zero. Such sensitivity peaks cannot be observed in the different publications and thus a further analysis is necessary. First such results can be reproduced with the different FEM models and method for finding the resonance condition. An interpretation can be done from the peak shape. From Equation (12), it is clear
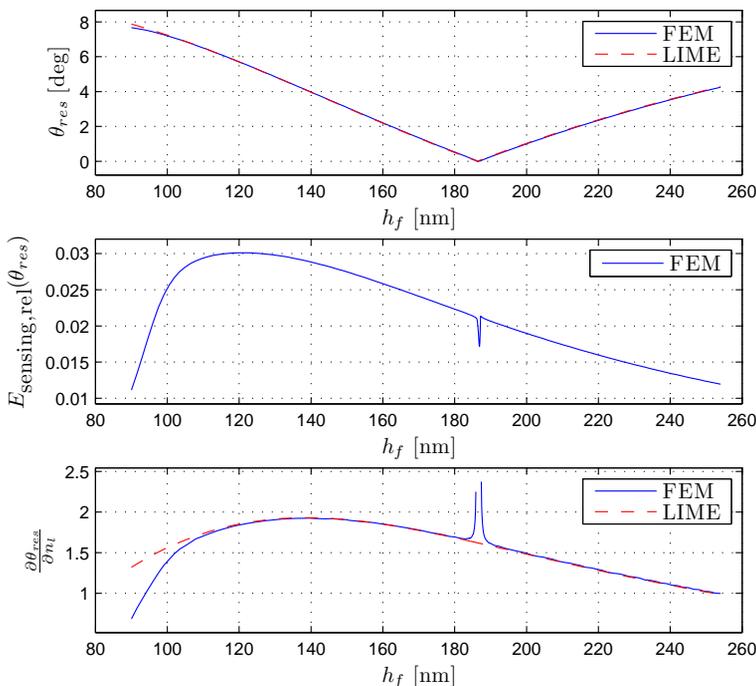
Figure 7. Sensitivity for different film thicknesses obtained with FEM and LIME.

that the resonance condition θ_{res} is not at θ_0. The derivative $\frac{\partial \theta_{\mathrm{res}}}{\partial \theta_0}$ is very big near the normal incidence, then a very small change of θ_0 can produces a very large change of the coupling condition. Far away from the origin the derivative is approximately equal to one because there is no influence between the two peaks. Since the sensitivity is linear in the region of the normal incidence, a reasonable hypothesis is that the angle θ_0 is locally linearly dependent with respect to the film thickness. With the above mentioned findings, it can be stated that the change of the coupling condition is no more linear but that a resonance peak occurs as expected from the FEM results because:

$$\frac{\partial \theta_{\mathrm{res}}}{\partial n_f} \sim \frac{\partial \theta_{\mathrm{res}}}{\partial \theta_0} \quad \text{where} \quad \theta_0 \sim n_f \tag{15}$$

This means that a part of the incident wave is coupled by the peak with the maximum at $+\theta_0$ and another part by the peak at $-\theta_0$. Consequently, a wave is coupled in both directions into the waveguide and therefore the energy in the waveguide is maximal at a point (or the
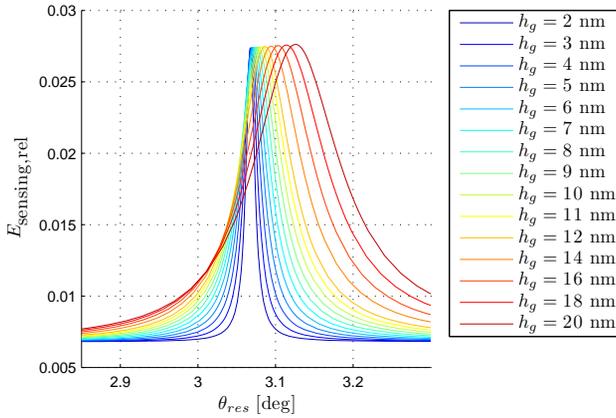
Figure 8. Resonance peaks (Lorentzian fits) for different grating depths.

transmission coefficient is minimal) where $\theta_{\mathrm{res}} \neq \theta_0$. This is obvious if the resonance is $\theta_{\mathrm{res}} = 0$ that there are waves in both directions. With a configuration with two pads (as shown in Figure 1), only one of the two waves can be used and thus the peak of the sensitivity curve does not appear (LIME simulation results).

5.2. Grating Depth

The grating depth has only a small influence over the resonance angle. The sensitivity variation is less than 1% for grating depth from 1 nm to 20 nm. The most important impact of the grating depth is on the full width half maximum of the resonance peak. This can be seen in Figure 8 where the complete peaks can be seen for several different grating depths.

A peak with a small full width half maximum is preferable because it allows an accurate detection of the resonance during the experiments. But since there are some tolerances due to the fabrication of the chip, the grating depth cannot be too small. The coupling efficiency is also smaller for a thin grating. Therefore the grating depth and duty cycle can be used as tuning parameters for the resonance peak shape. These parameters are decoupled since there is no influence on the resonance position or on the sensitivity. Even if the grating is geometrically shallow, the grating depth should be considered for finding the sensor response. The grating depth is not the only parameter which has an influence on the peak width, the number of periods [6, 17] and the losses have also a significant impact.

5.3. Film Losses

The losses in the cover and the substrate have less influence on the sensor response than the film losses. A complex refractive index is used where the imaginary part is the extinction coefficient k. The problem is to find an adequate value for the extinction coefficient. Measurements are possible (for example with prism couplers or ellipsometry) but were not available for the used chip. It is very hard to find a value in the different publications because the extinction coefficient is strongly dependent on the production process used for the chip (temperature, pressure and film thickness) and on the frequency.

For a Ta_2O_5 chip, the described k-values are varying between $< 10^{-4}$ [20] and 0.02 [1]. As explained in [20], there are also losses at the substrate-film and the film-cover interface. A resulting value of $k = 0.001$ has been chosen for the simulation and the resulting peak for the transmission coefficient and total field are computed. With the losses the full width half maximum is no more $0.001°$ but about $0.045°$. The results are exactly the same with the scattered field formulation. Consequently an accurate measurement of the losses would be required to faithfully simulate the resonance peak. The resonance position is not strongly dependent of the losses (less than $0.001°$). This implies that the sensitivity can be computed with the model without losses as done above.

6. CONCLUSIONS

A new algorithm, based on FEM, TLTMM (Transmission Line Transfer Matrix Method) and model-based search, has been presented for finding the sensitivity of a grating based dielectric biosensor. The proposed FEM-based solution scheme has proven his validity against the Local Interference Method (LIME). Particularly the limits of the LIME method for large grating depths have been shown. For thin gratings, the two methods are in very good agreement. The error between the different numerical methods for the position of the resonance angle is smaller than $10^{-5°}$.

The presented application examples show that the influence off the grating depth and the film losses can be neglected for the computation of the resonance position or the sensitivity. In the other hand, the impact of these factors on the resonance peak shape (full width half maximum).

A more complex method also exists for the simulation of band gap dielectric frequency-selective surfaces [21]. A similar method combined with the proposed procedure for obtaining the sensitivity could lead

to a faster algorithm. Another solution would be to use the multiple scattering approach [9].

Extension of the method for aperiodic grating or for including surface roughness has been done with success (total field or scattered field combined with TLTMM). The only difference for aperiodic gratings is that PMLs are added instead of Floquet periodicity. For the total field formulation, the mode equation is solved (without the grating) and the results are set as the injection boundary condition (simulation of an output coupler). The total field model could probably be adapted to compute more complex excitations than a plane wave.

Thus most of the sensor parameters can be taken into account and a global optimization of the chip is possible with a procedure that is rather easy to implement with the help of standard simulation software. Since one the key advantage of grating based biosensors is the important number of tuning parameter, it is crucial to be able to simulate the impact of each variable for the design.

REFERENCES

1. Schmitt, K., K. Oehse, G. Sulz, and C. Hoffmann, "Evanescent field sensors based on tantalum pentoxide waveguides — A review," *Sensors*, Vol. 8, 711–738, Feb. 2008.

2. Schmitt, K. and C. Hoffmann, "High-refractive-index waveguide platforms for chemical and biosensing," *Optical Guided-wave Chemical and Biosensors I*, Vol. 7, 21–54, 2009.

3. Cottier, K., "Advanced label-free biochemical sensors based on integrated optical waveguide gratings," Ph.D. Thesis, Université de Neuchâtel, May 2004.

4. Cottier, K., M. Wiki, G. Voirin, H. Gao, and R. Kunz, "Labelfree highly sensitive detection of (small) molecules by wavelength interrogation of integrated optical chips," *Sensors and Actuators B: Chemical*, Vol. 91, Nos. 1–3, 241–251, 2003.

5. Kunz, R. and K. Cottier, "Optimizing integrated optical chips for label-free (bio-) chemical sensing," *Analytical and Bioanalytical Chemistry*, Vol. 384, 180–190, Dec. 2005.

6. Kunz, R., J. Dübendorfer, and R. Morf, "Finite grating depth effects for integrated optical sensors with high sensitivity," *Biosensors and Bioelectronics*, Vol. 11, Nos. 6–7, 653–667, 1996.

7. Tiefenthaler, K. and W. Lukosz, "Sensitivity of grating couplers as integrated-optical chemical sensors," *JOSA B*, Vol. 6, 209–220, Oct. 1989.

8. Cottier, K., R. Kunz, and H. Herzig, "Efficient and practical

modeling of finite waveguide grating couplers," *Japanese Journal of Applied Physics*, Vol. 43, 5742–5746, Aug. 2004.

9. Moreno, E., D. Erni, C. Hafner, R. Kunz, and R. Vahldieck, "Modeling and optimization of non-periodic grating couplers," *Optical and Quantum Electronics*, Vol. 34, No. 11, 1051–1069, 2002.

10. Chen, C. L., *Foundations for Guided-Wave Optics*, Wiley, 2006.

11. Palmer, C. and T. Rgl, *Diffraction Gratings and Applications*, Marcel Dekker, 1997.

12. COMSOL, *Plasmonic Wire Grating*, Apr. 2011, http://www.comsol.com/showroom/gallery/10032.

13. Fernandez, F. and Y. Lu, *Microwave and Optical Waveguide Analysis by the Finite Element Method*, John Wiley & Sons, 1996.

14. COMSOL, *RF Module User's Guide*, Oct. 2011, http://comsol.com.

15. Oraizi, H. and M. Afsahi, "Analysis of planar dielectric multilayers as FSS by transmission line transfer matrix method (TLTMM)," *Progress In Electromagnetics Research*, Vol. 74, 217–240, 2007.

16. Oraizi, H. and M. Afsahi, "Transmission line modeling and numerical simulation for the analysis and optimum design of metamaterial multilayer structures," *Progress In Electromagnetics Research B*, Vol. 14, 263–283, 2009.

17. Brazas, J. and L. Li, "Analysis of input-grating couplers having finite lengths," *Appl. Opt.*, Vol. 34, 3786–3792, Jul. 1995.

18. Maron, M., *Numerical Analysis: A Practical Approach*, Collier Macmillan, 1982.

19. Horvath, R., L. Wilcox, H. Pedersen, N. Skivesen, J. Hesthaven, and P. Johansen, "Analytical and numerical study on grating depth effects in grating coupled waveguide sensors," *Applied Physics B: Lasers and Optics*, Vol. 81, No. 1, 65–73, 2005.

20. Esboubas, L., S. Tisserand, and A. Gatto, "Le bilan des pertes dans les couches minces optiques par mesures d'absorption et d'atténuation à la propagation guidée," *Journal of Optics*, Vol. 29, No. 1, 40, 1998.

21. Coves, A., B. Gimeno, M. Andres, A. Blas, V. Boria, and J. Morro, "Analysis and applications of dielectric frequency-selective surfaces under plane-wave excitation," *IEEE Antennas and Propagation Society International Symposium*, Vol. 2, 825–828, June 2003.